agronomy

MDPI

Article

Contrasting Decomposition Dynamics of Absorptive and Transport Roots of Cotton Under Different Nitrogen Fertilization Rates

Yunzhu He [1], Zihui Shen [1,2], Mengjuan Liu [1], Xiaoxiao Liu [1], Hushan Wang [1], Qian Zhang [1], Wangfeng Zhang [2,*] and Xiaozhen Pu [1,*]

[1] Xinjiang Production and Construction Corps Key Laboratory of Oasis Town and Mountain-Basin System Ecology, College of Life Sciences, Shihezi University, Shihezi 832000, China; 20232006027@stu.shzu.edu.cn (Y.H.)
[2] Key Laboratory of Oasis Eco-Agriculture of Xinjiang Corps, College of Agriculture, Shihezi University, Shihezi 832000, China
* Correspondence: zhwf_agr@shzu.edu.cn (W.Z.); puxz2016@shzu.edu.cn (X.P.); Tel.: +86-13999332625 (W.Z.); +86-18116845525 (X.P.); Fax: +86-09932057990 (W.Z.); +86-09932057262 (X.P.)

Abstract

Root litter decomposition is key to terrestrial nutrient cycling, yet how functionally divergent roots respond to nitrogen (N) addition remains unclear. We compared absorptive roots (AR) and transport roots (TR) in an 80-day in situ litterbag experiment in an arid oasis cotton field under four N rates (N0, 0; N1, 231; N2, 280.5; N3, 330 kg·ha^{-1}). N addition regulated the two root types differently. AR decomposition peaked under moderate N supply (N2) with weakened stimulation at N3, whereas TR decomposition increased continuously with N rate. AR rapidly released labile carbon and phosphorus but immobilized N; TR showed sustained net N release under high N (32.9–46.6%). Principal component analysis of eight litter traits identified a decomposition economics spectrum along the first axis (57.0% of variance), from a fast-decomposition end (high SRL, N, P) to a conservative end (high cellulose, C, AD, RTD). PC1 scores differed between root types and N treatments and correlated positively with decomposition rate. AR shifted toward the fast end under moderate N supply, whereas TR remained at the conservative end. Hierarchical partitioning linked AR decomposition mainly to morphological dynamics (47.7%) and TR decomposition to climatic factors (54.2%). Structural equation modeling indicated that N addition affected decomposition indirectly through soil pathways, via morphological traits in AR and nutrient mineralization in TR. Root functional identity thus shapes the decomposition strategies and driving pathways of cotton root litter, providing new perspectives for N management.

Keywords: absorptive roots; transport roots; litter decomposition; nutrient cycling; nitrogen application; cotton

Check for updates

Academic Editor: Alfonso Albacete

Received: 8 October 2026
Revised: 12 November 2026
Accepted: 16 November 2026
Published: 18 November 2026

Copyright: © 2026 by the authors. Licensee MDPI, Basel, Switzerland. This article is an open access article distributed under the terms and conditions of the Creative Commons Attribution (CC BY) license.

1. Introduction

Plant litter decomposition is a central process in terrestrial nutrient cycling. It directly regulates soil carbon dynamics and plant nutrient availability, thereby maintaining ecosystem functioning and stability [1,2]. The rate and pattern of litter decomposition depend on intrinsic litter properties, including initial chemical composition, anatomical structure, and functional traits. These properties essentially reflect the plant trade-off between resource acquisition investment and tissue construction costs [3]. The root economics spectrum (RES) provides a systematic framework for understanding such functional trade-offs in

living roots, but it primarily concerns resource acquisition and physiological maintenance during the active life stage [4]. Plant functional traits are increasingly recognized to exert carry-over effects on decomposition after tissue death. Freschet et al. [5] conducted a multi-organ decomposition experiment and found that the predictive capacity of the RES for decomposition was unstable. They therefore proposed the decomposition economics spectrum (DES), a plant economics spectrum of litter decomposability distinct from the RES. Birouste et al. [6] further confirmed that root decomposition rate cannot be explained by morphological traits alone. Thus, although the RES and the DES are linked through trait carry-over effects, the predictive power of these effects is unstable. The acquisition-conservation trade-off underlying the living root economics spectrum cannot be directly extrapolated to the decomposition stage, and root decomposition may follow a distinct regulatory logic that involves chemical traits. Overall, the DES framework remains at the stage of conceptual development. Existing studies have examined the association between root traits and decomposition dynamics, but their results are inconsistent and mostly based on interspecific comparisons or mixed root samples. Empirical evidence that couples morphological trait dynamics with decomposition processes at the scale of functional root types within a single species remains to be established.

Roots differ markedly in physiological function depending on their position of attachment within the root system, giving rise to root order classification theory [7,8]. Although the correspondence between root order and function varies among plant species, this classification framework has been validated in a variety of woody and herbaceous species [9,10]. According to this theory, any in-depth study of roots should be grounded in root order classification. Lower-order roots at the distal ends of the root system function as absorptive roots (AR), whereas higher-order roots function as transport roots (TR) [9,11]. AR generally exhibit higher specific root length (SRL) and nitrogen content and have a shorter lifespan, whereas TR exhibit higher tissue density and lignin content and have a longer lifespan [10,12]. This fundamental divergence in anatomical structure and chemical composition indicates that the two root types follow distinct decomposition trajectories and fates at the litter stage [13]. For example, Yin et al. [14] suggested that AR, owing to their soft tissues and low investment in defensive compounds, show high mass loss rates at the early decomposition stage and release a large pulse of labile nitrogen and phosphorus within a short period. In contrast, TR possess well-developed secondary structures, are rich in recalcitrant phenolic compounds, and decompose slowly. Their recalcitrant residues persist longer in soil and are regarded as a potential source of the stable soil organic carbon (SOC) pool [15,16].

Nitrogen fertilization is one of the most critical management practices in agroecosystems. Once applied to the soil, nitrogen regulates root litter decomposition through a cascade of direct and indirect effects [17]. These effects occur at two stages, before and during decomposition. Before decomposition, nitrogen input directly regulates litter substrate quality by altering plant carbon allocation, thereby modifying initial nitrogen content, C/N ratio, and lignin content [18]. During decomposition, nitrogen input modifies the decomposition microenvironment by changing soil physicochemical properties such as pH and aggregate stability and profoundly affects microbial metabolic strategies, biomass, and extracellular enzyme activities [19,20]. Moreover, these two pathways often act synergistically. For instance, excessive nitrogen application not only lowers the root C/N ratio but also alters the rhizosphere microenvironment. This may trigger microbial stoichiometric imbalance and shift microbial decomposition pathways, ultimately influencing the fate of root-derived carbon and nutrient cycling efficiency [21–23]. The recovery of applied nitrogen by crops is low. Its fate depends not only on plant nitrogen uptake during the current season but also on when and how rapidly the nitrogen retained in root residues

re-enters the soil nutrient cycle. Differences in the turnover and decomposition of roots with different functional identities therefore influence the temporal pattern and total amount of apparent fertilizer nitrogen recovery [24]. Therefore, treating roots as a homogeneous structure while ignoring their functional heterogeneity may obscure the mechanisms by which nitrogen application regulates nutrient return and weaken the targeting of nitrogen fertilizer management. Elucidating the responses of functionally distinct roots to nitrogen input and the cascading effects of their decomposition provides a new decomposition-based perspective for optimizing fertilizer management and maintaining ecosystem sustainability in agroecosystems [25].

Xinjiang in northwestern China is a globally important cotton-producing region [26], where cotton production relies heavily on drip irrigation. Drip irrigation effectively regulates the hydrothermal conditions of the root zone and provides relatively stable microsite conditions for crop growth and soil biological processes. However, long-term heavy nitrogen inputs, coupled with the localized enrichment effect of drip irrigation, have led to pronounced nitrogen accumulation alongside slow nutrient turnover in cropland soils [27,28]. Cotton is a typical annual crop with active root metabolism throughout its growth cycle. After harvest, large quantities of root residues are returned to the soil, constituting an important source of belowground carbon and nutrient inputs in croplands [29,30]. This field scenario, with long-term high nitrogen input and localized enrichment, provides typical conditions for examining the decomposition divergence between functional root types under nitrogen gradients. In a previous study, our group systematically classified the cotton root system [31]. First- to third-order roots lack secondary development, have a well-developed cortex, and serve absorptive functions. Fourth- to fifth-order roots exhibit well-developed secondary xylem and serve transport and support functions. The two root groups can be reliably distinguished by morphological, anatomical, and physiological traits. However, the decomposition of these two functional root types remains insufficiently understood. On the one hand, evidence for root decomposition under the DES framework is mostly derived from interspecific comparisons or mixed root samples, and empirical studies at the level of functional root types within a single species remain to be expanded. On the other hand, how nitrogen application differentially regulates the decomposition of the two root types and how substrate traits interact with soil and climatic conditions to jointly drive their decomposition still require systematic quantitative analysis. Accordingly, we conducted a controlled decomposition experiment to investigate how nitrogen application regulates litter decomposition and nutrient release of the two functional root types. By integrating the DES framework with root order functional classification, we quantified the decomposition rates, nutrient release, and multi-level driving pathways of the two root types under a nitrogen gradient. This study aims to provide a new perspective based on root decomposition for elucidating the mechanisms of belowground nutrient return in agroecosystems and optimizing fertilization management. We hypothesized that (1) based on the divergence in functional identity, the decomposition strategies of AR and TR are expected to diverge, and the covariation of their decomposition traits can potentially be characterized by the DES, with AR approaching the fast-decomposition end of the spectrum axis and TR approaching the structurally conservative end; (2) the two root types may differ in their response pathways to nitrogen application, such that AR with higher substrate quality respond already under moderate nitrogen addition while the promoting effect of excessive nitrogen tends to weaken, whereas TR, which experience stronger nitrogen limitation, may show a clear response only under high nitrogen input; and (3) this divergence may further extend to the driving mechanisms, with AR decomposition expected to be regulated more by morphological trait dynamics and TR decomposition constrained more by hydrothermal

conditions and nutrient supply, while nitrogen application may affect the decomposition of both root types mainly through indirect effects mediated by the soil environment.

2. Materials and Methods

2.1. Experimental Site

The experiment was conducted at the Agricultural Experimental Station of Shihezi University, Shihezi City, Xinjiang Uygur Autonomous Region, China (86°01′42″ E, 44°29′40″ N). The region has a temperate continental arid climate, with a mean annual temperature of 7 °C, annual precipitation of 209 mm, annual evaporation of 1659 mm, annual sunshine duration of 2859.2 h, and a frost-free period of approximately 175 d. The soil is a grey desert soil with a loamy texture, classified as a Calcisol in the World Reference Base for Soil Resources. The machine-harvested cotton cultivar Xinluzao 84 (Xinjiang Hexin Seed Co., Ltd., Shihezi, China) was sown on 22 April 2024 and harvested on 5 October 2024. Cotton was grown under a drip-irrigation-under-mulch system with one plastic film, three drip tapes, and six rows per film, at a row spacing of (66 + 10) cm, a plant spacing of 10 cm, and a planting density of 280,000 plants·ha^{-1}. During the growing season, cotton was irrigated ten times at intervals of 7–9 d, with a total irrigation amount of 4124–4650 m^3·ha^{-1}. Nitrogen fertilizer (urea, $CO(NH_2)_2$, N ≥ 46.0%; Xinjiang Zhongneng Wanyuan Chemical Co., Ltd., Manas, China) was applied in split doses with the irrigation water, together with potassium dihydrogen phosphate (KH_2PO_4, 250 kg·ha^{-1}, containing 52% P_2O_5 and 34% K_2O; Sichuan Shengfeng Phosphorus Chemical Co., Ltd., Shifang, China). Except for the nitrogen treatments, all other field management practices (irrigation, tillage, chemical weed and pest control, growth regulation and defoliation) were identical across all plots in timing, frequency, and rate, following local commercial cotton production. On the day of litterbag deployment (day 0), soil was sampled from the 0–10 cm layer at five points within the quadrat of each plot using a soil auger, and the five subsamples were combined into one composite sample per plot. After roots and gravel were removed with a 2 mm sieve, the samples were used to determine the initial soil physicochemical properties and enzyme activities before decomposition. Each plot served as an independent replicate ($n = 3$). The basic physicochemical properties of the soil in each plot are summarized in Table 1.

Table 1. Initial soil chemical properties of the experimental plots under four nitrogen treatments.

NT	Soil Organic Carbon (g·kg^{-1})	Soil Total Nitrogen (g·kg^{-1})	Soil Total Phosphorus (g·kg^{-1})	SEI
N3	12.18 ±0.09	1.30 ±0.00	3.85 ±0.06	0.70 ±0.05
N2	13.77 ±0.10	1.32 ±0.00	3.46 ±0.04	0.95 ±0.01
N1	14.09 ±0.09	1.32 ±0.00	2.85 ±0.22	0.91 ±0.03
N0	14.13 ±0.08	1.24 ±0.00	1.73 ±0.05	0.90 ±0.03

Note: Data are the initial soil chemical properties of the 0–10 cm layer in the experimental plots under different nitrogen (N) treatments, measured on the day of litterbag deployment (day 0), before the decomposition period started. Values are means ± standard error ($n = 3$). N0, N1, N2, and N3 represent N application rates of 0, 231, 280.5, and 330 kg·ha^{-1}, respectively. NT, nitrogen treatment; SEI, soil enzyme activity index calculated from the activities of urease, sucrase, and β-glucosidase. No plot-level soil measurements were taken before treatment establishment; therefore, the day-0 values represent the soil status at the start of decomposition and may reflect both the effects of the growing-season treatments and pre-existing variation.

2.2. Experimental Design and Treatment

This study used a single-factor randomized complete block design with four nitrogen treatments: conventional nitrogen application (N3, 330 kg·ha^{-1}), mild nitrogen reduction (N2, 280.5 kg·ha^{-1}, 15% reduction), moderate nitrogen reduction (N1, 231 kg·ha^{-1}, 30% reduction), and no nitrogen application (N0, 0 kg·ha^{-1}). All N rates are expressed as elemental N per hectare. The experiment comprised three blocks, each containing one plot per nitrogen treatment (12 plots in total), with treatments randomly assigned to plots within each block. Each plot measured 19 m × 6.3 m, and each nitrogen treatment was therefore replicated in three independent plots ($n = 3$). The N3 rate has been the conventional nitrogen application rate for cotton under drip irrigation with plastic film mulch in this region over the past decade. The 15% reduction (N2) was designed to evaluate the effect of mild nitrogen reduction approaching the agronomically optimal rate, whereas the 30% reduction (N1) was used to examine whether root decomposition under moderate nitrogen reduction could maintain nutrient turnover efficiency comparable to that under conventional nitrogen application. The 15% interval between the two reduction levels is sufficient to distinguish the differences in soil microbial activity and enzyme kinetics between nitrogen reduction intensities [32]. According to Ren et al. [33], the growth rates of cotton taproots and lateral roots peak between May and July, after which root mortality begins and the root system enters a period of rapid turnover. Based on the local cotton growth calendar, root samples were collected in situ from the 0–10 cm soil layer in mid-July 2024 at the full-bloom stage. Within each plot, the collected roots were thoroughly mixed into one composite sample per plot, and samples were not mixed across plots within the same nitrogen treatment, so that each plot constituted an independent biological replicate. Roots were transported to the laboratory and rinsed with deionized water to remove adhering soil; visibly dead roots were discarded. Roots were then classified according to the root-order classification method of Pregitzer et al. [7,34,35]. The most distal unbranched roots were defined as first-order roots, and their parent roots were successively designated as second-order, third-order, and up to fifth-order roots. Based on the previous findings of Dong et al. [31], in the same cotton system, first- to third-order roots were combined as AR and fourth- to fifth-order roots as TR. Roots of each type were cut into 4–5 cm segments and oven-dried at 65 °C to constant weight. One portion of the root samples was used for the subsequent decomposition experiment, and the remaining portion was used to determine the initial properties of the root litter.

Root samples (1.5 g) were placed in 100-mesh nylon litterbags (15 cm × 20 cm, mesh size ≈ 150 μm) for the decomposition experiment. This mesh size prevented the ingrowth of living roots while minimizing the loss of fine particulate matter during the later stages of decomposition. Within each plot, one 5 m × 5 m quadrat was established for the decomposition experiment, and a 3 m buffer strip was maintained between adjacent quadrats. To exclude interference from living roots and their exudates, all plants and surface residual roots within the quadrats were removed. The litterbags were placed horizontally and randomly at a soil depth of 5 cm in the corresponding nitrogen treatment plots [36] and covered with in situ soil. A total of 120 litterbags were prepared for each nitrogen treatment (2 root types × 4 sampling dates × 5 bags per root type per date × 3 replicate plots), giving 480 bags in total, and the initial samples were not enclosed in litterbags. At 20, 40, 60, and 80 days after deployment, five AR bags and five TR bags, together with the surrounding soil, were retrieved from each of the three replicate plots of each treatment. After each sampling, the five AR bags and the five TR bags retrieved from the same plot were each combined into one composite litter sample, and the soil surrounding the ten bags from the same plot was combined into one composite soil sample per plot. Samples from different blocks of the same nitrogen treatment were not mixed. The three blocks therefore provided three

independent composite replicates per treatment at each sampling date. At each sampling, the litter samples were rinsed with clean water, oven-dried to constant mass, and weighed.

2.3. Indicator Determination

The measured indicators included root litter and soil-related parameters.

For root litter, N content was determined by the Kjeldahl method, C content by the potassium dichromate volumetric method with external heating, and P content by the vanadium-molybdate yellow colorimetric method [37]. Total non-structural carbohydrates (TNC) and cellulose contents were determined by the anthrone colorimetric method [38,39], and lignin content by the Klason method [40]. Root morphological traits were determined by scanning the root samples into images with a root scanner (Epson Expression 10000XL; Seiko Epson Corp., Nagano, Japan), and the resulting images were analyzed for root morphological parameters using WinRHIZO Pro 2013e (Regent Instruments Inc., Quebec City, QC, Canada).

The decomposition rate (K) of roots was calculated according to the exponential decay model of Olson (1963) [41]:

$$K = -\frac{\ln(X_t/X_0)}{\mathrm{t}} \quad (1)$$

where X_0 and X_t are the initial and final masses of the sample, respectively, and t is time in days [42]. The litter nutrient release rate (ΔY) was calculated as follows:

$$\Delta Y(\%) = \frac{M_0C_0 - M_tC_t}{M_0C_0} \times 100 \quad (2)$$

where M_0 and M_t represent the dry mass of litter at time 0 and at time t, respectively; C_0 and C_t represent the concentration of a given nutrient in litter at time 0 and at time t, respectively; $\Delta Y > 0$ indicates net release; $\Delta Y < 0$ indicates net enrichment. The soil enzyme activity index (SEI) was calculated as follows. To avoid interference from negative values in the subsequent weighted summation, the raw activity data of urease, sucrase, and β-glucosidase were first subjected to MAX normalization to eliminate dimensional differences. Objective weighting based on principal component analysis (PCA) was then applied: PCA was performed on the standardized matrix, the loading coefficients (l_i) of the first principal component (PC1) were extracted, and the weight of each enzyme was calculated by normalizing the absolute values of the loadings:

$$\omega_\mathrm{i} = \frac{|l_\mathrm{i}|}{\sum_{\mathrm{i}=1}^{\mathrm{n}}|l_\mathrm{i}|} \quad (3)$$

$$\mathrm{SEI} = \sum_{\mathrm{i}=1}^{\mathrm{n}} \omega_\mathrm{i} \times z_\mathrm{i} \quad (4)$$

where $\omega_\mathrm{i}\omega_\mathrm{i}$ represents the weight of soil enzyme activity (i), and $\mathrm{z_i}\mathrm{z_i}$ represents the MAX-normalized enzyme activity value.

2.4. Statistics and Analysis

All analyses were conducted on plot-level composite samples, and the individual plot ($n = 3$ independent plots per treatment), rather than the individual litterbag, was treated as the experimental unit. A three-way ANOVA tested the effects of root type (RT), nitrogen treatment (NT), sampling time (T), and their interactions on residual biomass (Figure 1, Table S1). Differences in residual biomass and in the release rates of TNC, C, N, P, cellulose and lignin (Figure 2), among sampling dates within each NT and among NTs within each date, were tested by one-way ANOVA followed by Duncan's multiple range test (SPSS Statistics 22.0). Prior to ANOVA, normality of model residuals was assessed with Shapiro–Wilk tests and homogeneity of variance with the median-centered Levene (Brown–Forsythe)

test; all assumptions were met ($p > 0.05$; Table S2). Principal component analysis (PCA) of the z-standardized litter trait matrix defined a decomposition strategy axis (PC1), and its association with *K* was tested with a linear mixed-effects model (Figure 3; Table 2; model details in Supplementary Methods S1). Nitrogen effects on *K* were evaluated with linear mixed-effects models, with temperature and precipitation included as covariates to account for the time-varying hydrothermal background, followed by Tukey-adjusted comparisons of estimated marginal means (Figure 4a; Table 3; Supplementary Methods S1). Hierarchical partitioning quantified the independent contributions of each factor group to the explained variation in *K* at the module scale (Figure 4b) and at the individual-trait scale (Figure 4c; Supplementary Methods S1). Piecewise structural equation models (piecewiseSEM) were fitted separately for the two root types, with all 16 variables grouped into four a priori modules (climate, soil, morphology and nutrient release) following a fully forward cascade; model adequacy was assessed by Fisher's C, submodel R^2, variance inflation factors and bootstrap resampling (Figure 5; Tables S11–S15; details in Supplementary Methods S1). Analyses used R v4.3.0 (lme4 v1.1-37, lmerTest v3.2-1, piecewiseSEM v2.3.0, relaimpo v2.2-7, emmeans v1.11.0); figures used ggplot2 v4.0.3 and patchwork v1.3.2. Meteorological data were obtained from the Mirror Earth platform.

Table 2. Linear mixed-effects model tests for PC1 scores and the decomposition rate (*K*).

Response Variable	Factor	NumDF	DenDF	F	*p*
PC1 score	RT	1	108	1940.32	<0.001 ***
	NT	3	108	29.77	<0.001 ***
	RT × NT	3	108	7.34	<0.001 ***
K	PC1	1	91	14.15	<0.001 ***
	RT	1	91	7.60	0.007 **
	PC1 × RT	1	89	1.54	0.218 ns

Note: PC1 scores were derived from a joint principal component analysis of eight z-standardized litter traits across all samples ($n = 120$). PC1 scores were modeled as a function of root type (RT), nitrogen treatment (NT) and their interaction; *K* was modeled as a function of PC1, RT and their interaction. Both models included sampling date as a random intercept. NumDF and DenDF are numerator and denominator degrees of freedom, with DenDF estimated by the Satterthwaite approximation. **, $p < 0.01$; ***, $p < 0.001$; ns, not significant.

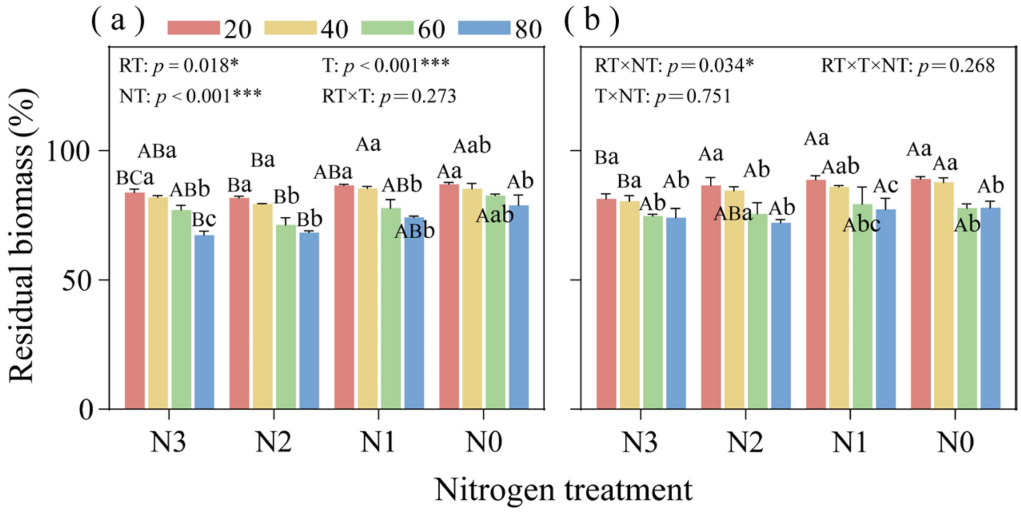


Figure 1. Residual biomass dynamics of absorptive (**a**) and transport roots (**b**) under nitrogen treatments. Data are means ± SE ($n = 3$). Different uppercase letters indicate significant differences among nitrogen treatments within the same sampling date, and different lowercase letters indicate significant differences among sampling dates within the same nitrogen treatment (one-way ANOVA

followed by Duncan's multiple range test, $p < 0.05$). The *p*-values shown in the panels are from the three-way ANOVA of root type (RT), sampling time (T), nitrogen treatment (NT) and their interactions. N0, N1, N2, and N3 represent nitrogen application rates of 0, 231, 280.5, and 330 kg·ha^{-1}, respectively. *, $p < 0.05$; ***, $p < 0.001$.

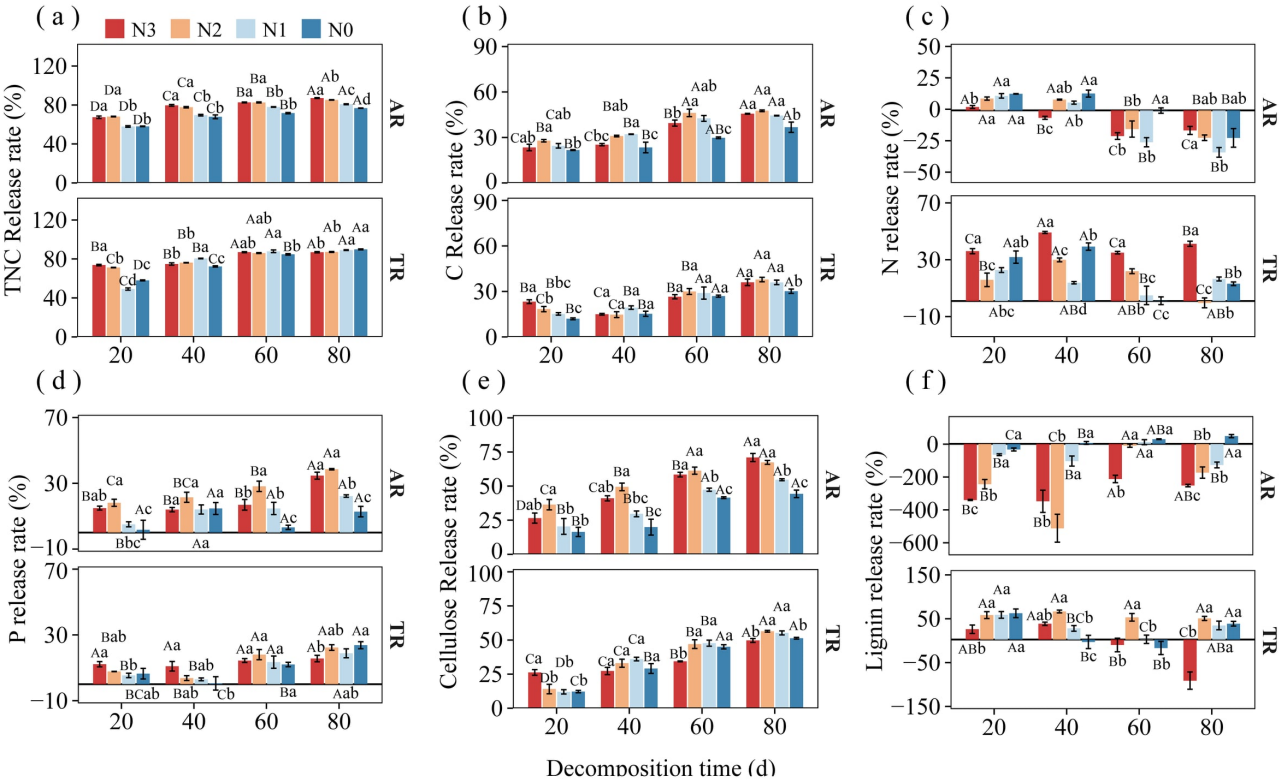


Figure 2. Release rates of total non-structural carbohydrates (TNC, (**a**)), carbon (**b**), nitrogen (**c**), phosphorus (**d**), cellulose (**e**) and lignin (**f**) in absorptive (AR) and transport roots (TR) under four nitrogen treatments during decomposition. Data are means ± SE ($n = 3$). Different uppercase letters indicate significant differences among decomposition times within the same nitrogen treatment, and different lowercase letters indicate significant differences among nitrogen treatments within the same decomposition time (one-way ANOVA followed by Duncan's multiple range test, $p < 0.05$). Positive values indicate net release and negative values indicate net enrichment (Equation (2)). N0, N1, N2, and N3 represent nitrogen application rates of 0, 231, 280.5, and 330 kg·ha^{-1}, respectively.

Table 3. Linear mixed-effects model tests for nitrogen and climatic effects on the decomposition rate (K).

Root Type	Factor	NumDF	DenDF	F	*p*
AR	NT	3	10	3.84	0.046 *
	Temperature	1	10	14.72	0.003 **
	Precipitation	1	10	11.98	0.006 **
TR	NT	3	10	1.99	0.179 ^{ns}
	Temperature	1	10	4.28	0.065 ^{ns}
	Precipitation	1	10	3.25	0.102 ^{ns}

Note: K was z-standardized and modeled separately for each root type, with nitrogen treatment (NT) as a fixed effect, temperature and precipitation as covariates, and the nitrogen treatment × sampling date combination as a random intercept. NumDF and DenDF are numerator and denominator degrees of freedom, with DenDF estimated by the Satterthwaite approximation. AR, absorptive roots; TR, transport roots. *, $p < 0.05$; **, $p < 0.01$; ns, not significant.

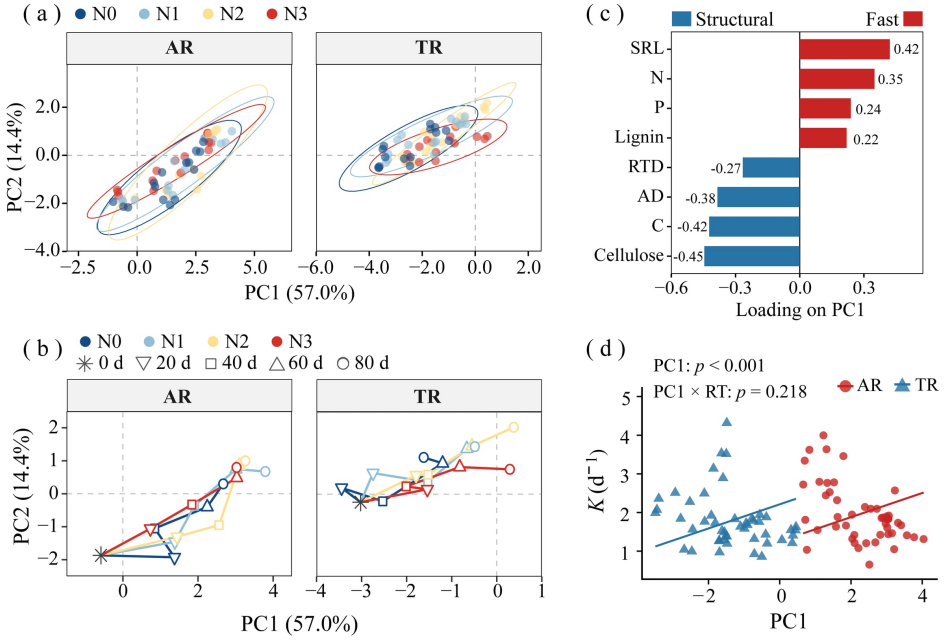


Figure 3. Joint principal component analysis of litter traits and its association with the decomposition rate. (**a**) Distribution of sample scores along PC1 and PC2 for absorptive (AR) and transport roots (TR) under four nitrogen treatments; ellipses indicate 95% confidence intervals. (**b**) Trajectories of mean PC1 and PC2 scores across decomposition time (0, 20, 40, 60 and 80 d) for each nitrogen treatment. (**c**) Loadings of the eight litter traits on PC1, defining the fast-decomposition end (positive loadings) and the structurally conservative end (negative loadings). (**d**) Relationship between PC1 scores and the decomposition rate (K); lines are fitted by a linear mixed-effects model with sampling date as a random intercept, and p-values for PC1 and the PC1 × RT interaction are shown. The PCA was performed on the combined z-standardized trait matrix of all 120 samples. N0, N1, N2, and N3 represent nitrogen application rates of 0, 231, 280.5, and 330 kg·ha^{-1}, respectively. SRL, specific root length; AD, average diameter; RTD, root tissue density; N, C and P, litter nitrogen, carbon and phosphorus contents.

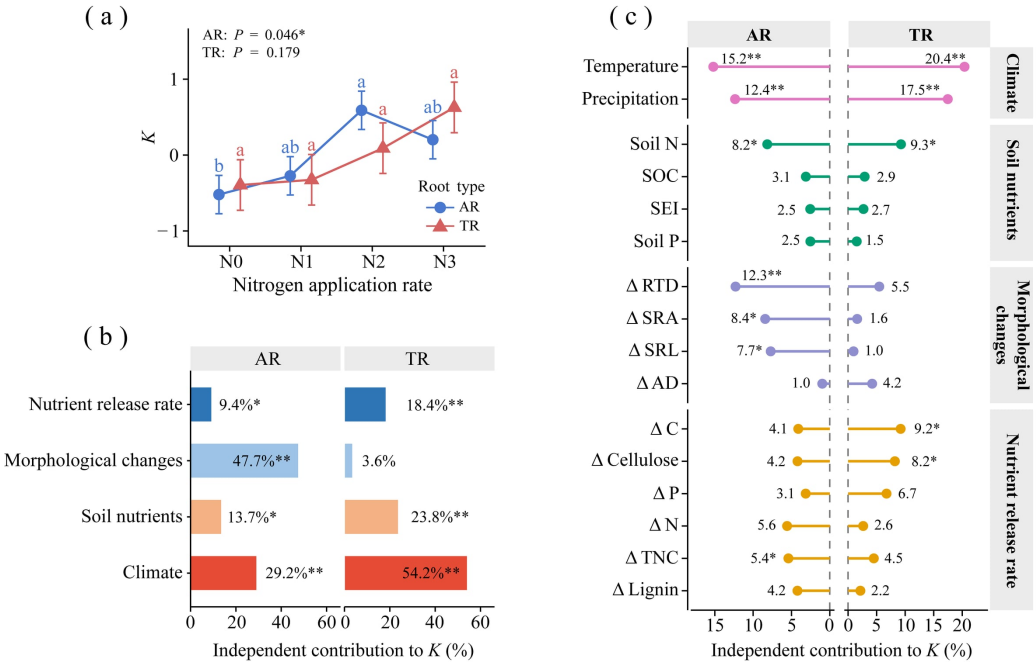


Figure 4. Nitrogen effects on the decomposition rate (K) and the relative contributions of driving factors to K in absorptive (AR) and transport roots (TR). (**a**) Estimated marginal means of z-standardized

K under four nitrogen treatments, from linear mixed-effects models fitted separately for each root type with temperature and precipitation as covariates. Data are means ± SE. Different lowercase letters indicate significant differences among nitrogen treatments within each root type (Tukey-adjusted comparisons, $p < 0.05$). The *p* values in the panel indicate the nitrogen treatment effect for each root type. (**b**,**c**) Independent contributions of driving factors to the explained variation in *K*, quantified by hierarchical partitioning at the module scale (**b**) and the trait scale (**c**). Significance was assessed by 999 permutations of the response variable. The Δ prefix denotes the change in a trait during decomposition. SOC, soil organic carbon; SEI, soil enzyme activity index; RTD, root tissue density; SRA, specific root area; SRL, specific root length; AD, average diameter; TNC, total non-structural carbohydrates. *, $p < 0.05$; **, $p < 0.01$; ns, not significant.

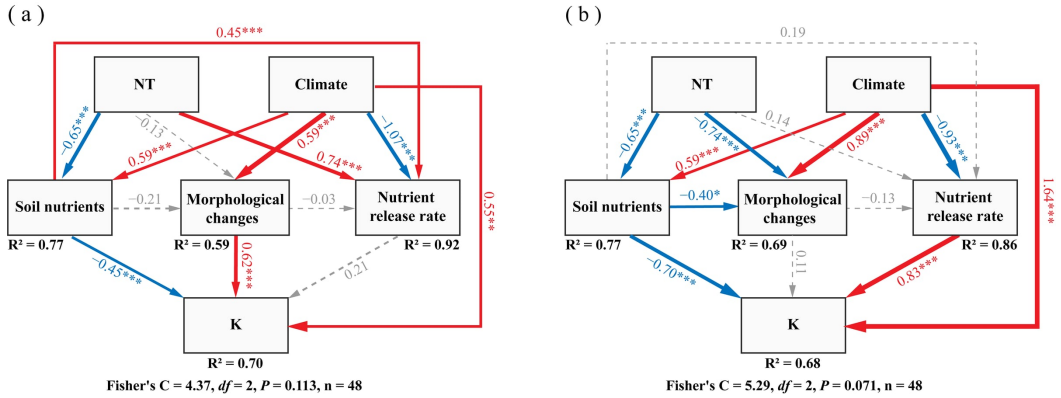


Figure 5. Piecewise structural equation models of the pathways regulating the decomposition rate (*K*) in absorptive (AR, (**a**)) and transport roots (TR, (**b**)). Numbers on arrows are standardized path coefficients, and line width is proportional to the absolute value of the standardized path coefficient. Red and blue arrows indicate positive and negative paths, respectively; solid arrows indicate significant paths and dashed arrows indicate non-significant paths. R^2 values below each box indicate the proportion of variance explained for that endogenous variable. Model fit was assessed by Fisher's C statistic, and indirect effects were estimated with 1000 bootstrap resamples (Table S13). NT, nitrogen treatment; Climate, temperature and precipitation; Soil nutrients, SOC, soil total N, soil total P and SEI; Morphological changes, ΔRTD, ΔSRA, ΔSRL and ΔAD; Nutrient release rate, ΔTNC, ΔC, ΔN, ΔP, ΔCellulose and ΔLignin; the Δ prefix denotes the change during decomposition. *, $p < 0.05$; ***, $p < 0.001$.

3. Results

3.1. Effects of Nitrogen Application on Litter Stoichiometry of Two Functional Root Types

The residual biomass of both root types decreased significantly with decomposition time ($p < 0.001$; Figure 1) and was significantly affected by root type ($p = 0.018$) and nitrogen treatment ($p < 0.001$), with a significant interaction between them ($p = 0.034$; Table S1). At day 80, the residual biomass of AR was significantly higher under N0 than under N2 and N3 (Figure 1a), whereas that of TR did not differ among the nitrogen treatments (Figure 1b). TNC was released rapidly from both root types (Figure 2a). In AR, release was consistently highest under N3, with significant treatment differences at day 80 ($p < 0.05$); in TR, it was higher under N3 and N2 than under N1 and N0 only at day 20, and the treatments converged thereafter. Carbon release at day 80 was significantly lower under N0 (36.7% in AR and 30.1% in TR) than under the nitrogen addition treatments ($p < 0.05$; Figure 2b). Nitrogen dynamics differed most strongly between the two root types (Figure 2c). AR shifted from slight net N release during the first 40 days to net N enrichment from day 60 onward; at day 80, enrichment was strongest under N1 (−32.9%) and significantly weaker under N3 (−15.7%, $p < 0.05$). TR under N3 maintained substantial net release throughout the decomposition period. Phosphorus was generally released from both root types (Figure 2d). At day 80, release in AR was significantly higher under N2 (38.5%) and N3 (34.6%) than

under N1 (22.2%) and N0 (12.8%); in TR, net release occurred from day 60 onward, with no significant treatment differences at day 80. Cellulose release increased continuously in both root types (Figure 2e). In AR, it was highest at day 80 under N3 (71.0%) and N2 (67.4%); in TR, the promotive effect of N3 (26.3%) was significant at day 20 but weakened thereafter, whereas release under N2 and N1 increased gradually. Lignin showed the most divergent pattern (Figure 2f). AR exhibited strong net enrichment that peaked under N2 at day 40 (−504.5%) and weakened thereafter; in TR, lignin was mainly released, with N2 maintaining net release throughout (47.5–63.0%) and N3 shifting to net enrichment from day 60 onward, reaching −92.2% at day 80.

3.2. Effects of Nitrogen Application on Decomposition of Two Functional Root Types

PCA was performed on the combined trait matrix of the two root types. Specific root area (SRA) was excluded prior to the analysis because of its strong collinearity with SRL ($r = 0.965$). PC1 explained 57.0% of the total trait variation and PC2 explained 14.4% (Figure 3, Table S3). The loading structure of PC1 reflected a trade-off in substrate quality along the DES (Figure 3c). The positive end of PC1 was defined mainly by SRL, N, P and lignin (loadings of 0.42, 0.35, 0.24 and 0.22, respectively), representing nutrient-rich, fast-decomposing substrates of high quality, and the positive loading of lignin reflected its relative enrichment during decomposition. The negative end was defined mainly by cellulose, C, average diameter (AD) and root tissue density (RTD) (loadings of −0.45, −0.42, −0.38 and −0.27, respectively), representing dense, slowly decomposing substrates of low quality. Linear mixed-effects models showed that *K* increased significantly with PC1 scores ($p < 0.001$; Table 2), and this relationship did not differ between the two root types (PC1 × RT interaction, $p = 0.218$; Figure 3d), indicating that PC1 serves as a decomposition strategy axis shared by both root types. Root type was the dominant source of variation in PC1 scores ($F = 1940.3$, $p < 0.001$), with AR consistently positioned at the fast-decomposition end and TR at the structurally conservative end (Figure 3a). Nitrogen treatment also significantly affected PC1 scores ($p < 0.001$), and its effect differed between the two root types (RT × NT interaction, $p < 0.001$). During decomposition, samples of both root types moved along PC1 toward the fast-decomposition end (Figure 3b), but their responses to nitrogen input differed. At day 80, PC1 scores of AR were higher under nitrogen addition than under N0 and peaked under N1 (2.67, 3.79, 3.26 and 3.03 under N0, N1, N2 and N3, respectively), consistent with the response of their decomposition rate. PC1 scores of TR increased with the nitrogen rate, remained at the structurally conservative end under N0 (−1.62) and N1 (−0.49), and shifted toward the fast-decomposition end only under N2 (0.38) and N3 (0.29).

3.3. Dominant Drivers of Decomposition Variation and Their Relative Contributions

Linear mixed-effects models (LMM-ANCOVA) showed that nitrogen application ($p = 0.046$), temperature ($p = 0.003$) and precipitation ($p = 0.006$) all significantly affected *K* in AR, whereas none of these effects was significant in TR (Table 3). After controlling for temperature and precipitation as covariates, nitrogen application significantly regulated *K* in AR (Figure 4a). *K* showed a unimodal response to increasing nitrogen rate, peaking under N2, and *K* under N0 was significantly lower than under N2 ($p < 0.05$). *K* of TR increased consistently with the nitrogen rate, but the differences among treatments were not significant. Module-level hierarchical partitioning showed that the dominant drivers of decomposition variation diverged between the two root types (Figure 4b, Table S8). In AR, the morphological change module had the largest independent contribution (47.7%, $p < 0.01$), followed by climate (29.2%, $p < 0.01$), soil nutrients (13.7%, $p < 0.05$) and nutrient release (9.4%, $p < 0.05$). In TR, climate was dominant (54.2%, $p < 0.01$), followed by soil nutrients (23.8%, $p < 0.01$) and nutrient release (18.4%, $p < 0.01$), whereas the morphological change

module contributed little and non-significantly (3.6%, $p > 0.05$). Single-layer partitioning of the 16 indicators further identified the specific regulating factors (Figure 4c, Table S9). In AR, the indicators with the largest independent contributions were temperature (15.2%), precipitation (12.4%) and ΔRTD (12.3%, all $p < 0.01$), and ΔSRA (8.4%), soil total N (8.2%), ΔSRL (7.7%) and ΔTNC (5.4%) also contributed significantly (all $p < 0.05$). In TR, the largest independent contributions came from temperature (20.4%, $p < 0.01$), precipitation (17.5%, $p < 0.01$), soil total N (9.3%, $p < 0.05$), ΔC (9.2%, $p < 0.05$) and ΔCellulose (8.2%, $p < 0.05$), whereas none of the morphological indicators contributed significantly.

4. Discussion

The regulatory effect of nitrogen application on cotton root decomposition varied with root functional identity. AR and TR exhibited systematic divergence in decomposition rate, nutrient release, and dominant driving pathways, and root functional identity was the key factor underlying this pattern.

4.1. Nutrient Release During Absorptive Root Decomposition and Its Regulation by Nitrogen

Across nitrogen treatments, AR litter showed a strong and sustained nutrient release response, with the regulatory effect of exogenous nitrogen persisting throughout decomposition. The TNC release rate of AR increased continuously with nitrogen application rate (Figure 2a), indicating that exogenous nitrogen input accelerated the leaching and mineralization of labile carbon fractions. On the one hand, nitrogen addition accentuated the characteristic morphology of AR, including high SRA, high SRL, and low AD (Figure S1), while increasing initial nitrogen content and decreasing the C/N ratio [43]. On the other hand, after AR entered the litter pool, their loose tissue structure could greatly facilitate microbial hyphal invasion and the diffusion of hydrolytic enzymes [44], and the availability of root metabolic residues increased accordingly [45,46]. During subsequent decomposition, rapid disintegration of parenchymatous cortical tissues further increased SRA and accelerated the degradation and turnover of labile components [47,48]. Consequently, AR became a preferentially utilized substrate for microbial catabolism [43,49] and were positioned toward the fast-decomposition end of the PC1 axis of the DES. The significant positive correlation between PC1 scores and *K* (Figure 3c,d) further gave this trait axis predictive capacity for decomposition rate across root types.

However, exogenous nitrogen did not regulate AR decomposition through a simple linear promotion effect. During early decomposition, AR were characterized by a high-nitrogen, low-carbon substrate with a low C/N ratio, which could theoretically supply sufficient nitrogen for microorganisms. In practice, exogenous nitrogen addition may have increased the likelihood that microorganisms preferentially assimilated and immobilized exogenous nitrogen [12]. One explanation based on previous studies is that adequate substrate nitrogen reduces microbial investment in nitrogen-acquiring enzymes and allows limited nitrogen resources to be reallocated to the synthesis and secretion of extracellular enzymes. For example, moderate nitrogen reduction has been reported to promote the synthesis and secretion of hydrolytic enzymes such as β-glucosidase, thereby accelerating litter carbon mineralization [50,51]. In contrast, excessive nitrogen input may indirectly constrain microbial utilization of complex carbon sources by inhibiting lignin-degrading enzyme activity or altering fungal community composition [52,53]. This mechanism was indirectly corroborated by the decomposition rate. Both the *K* value and the day-80 PC1 score of AR peaked under moderate nitrogen addition and declined under high nitrogen (Table S7; Figure 3b). This pattern suggests that excessive exogenous nitrogen offsets the decomposition advantage conferred by high substrate quality, possibly by disrupting microbial stoichiometric balance or inhibiting the activity of key extracellular enzymes.

Meanwhile, lignin was enriched in AR during early decomposition, and this enrichment was further intensified by exogenous nitrogen input [54,55]. These results indicate that nitrogen addition accelerates the consumption of labile carbon fractions while promoting the relative accumulation of recalcitrant components in the residue. This cascading shift in substrate chemical composition not only altered the decomposition rate of AR litter, but its potential effects on subsequent decomposition stages and on the long-term stability of SOC also warrant further examination in long-term observations. The high decomposition rate of AR and their sensitive response to moderate nitrogen input are consistent with the established view that the decomposition of high-quality litter is regulated by substrate stoichiometry. However, this nonlinear response indicates that the negative effect of excessive nitrogen remains evident even for high-quality substrates.

4.2. Nutrient Release During Transport Root Decomposition and Its Regulation by Nitrogen

The decomposition rate and nutrient release of TR generally lagged behind those of AR, whereas TR showed a distinctive sustained response to high nitrogen input. TR primarily function in nutrient conduction and mechanical support. Their dense, lignified stele and sclerenchymatous tissues form a robust physical barrier that tightly encases structural carbon skeletons such as cellulose, substantially increasing resistance to microbial enzymatic degradation [9]. This anatomical structure explains why TR maintained high AD and slow TNC release throughout decomposition and why their initial morphological traits responded weakly to nitrogen treatments (Figure S1). Consistent with this, morphological changes explained only 3.6% of the decomposition variation (Figure 4b). Because TR are rich in structural polysaccharides and have a high initial C/N ratio, their decomposition is inherently constrained by nitrogen limitation on enzyme synthesis [56]. Continuous exogenous nitrogen input effectively alleviated this stoichiometric constraint and significantly promoted the enzymatic degradation of cellulose during early decomposition [57,58]. Under the N3 treatment, TR exhibited sustained net nitrogen release and the highest *K* value (Figures 2c and 4a). The structural equation model further showed that nitrogen addition affected TR decomposition through an indirect path via the soil module (Table S13). The early nitrogen release from TR was temporally complementary to the nitrogen enrichment in AR during early decomposition. This complementarity may help relieve microbial competition for soil inorganic nitrogen pools and may sustain nutrient supply after the peak decomposition period of AR [59,60].

The promotion of TR decomposition by high nitrogen was also reflected in the coordination between morphological dynamics and driving factors. Under the N3 treatment, SRA and SRL of TR increased significantly during the middle decomposition stage, followed by a marked decline in RTD at the later stage (Figure S1). Hierarchical partitioning and the structural equation model consistently indicated that TR decomposition was governed primarily by the climatic background. Among root and soil factors, cellulose release and soil nitrogen supply were dominant (Figure 4b,c). These results suggest that high nitrogen input may have relieved the nutrient limitation on the synthesis of enzymes that degrade recalcitrant substrates [61]. High nitrogen input may also have enhanced the microbial capacity to decompose recalcitrant carbon by altering the functional structure of microbial communities [62]. These changes may in turn have promoted substantial enzymatic degradation and structural loosening of the lignin-encased cellulose skeleton, driving the decomposition rate to its maximum. However, under sustained high nitrogen input, lignin shifted from net release during the middle stage to net enrichment during the later stage (Figure 2f). This shift indicates that lignin-degrading enzyme activity was suppressed, which hindered the enzymatic degradation of the recalcitrant carbon skeleton and delayed the physical disintegration of the substrate structure. Meanwhile, the mineralization of native soil organic

nutrients and the release of labile nitrogen increased concurrently (Figure S2). This pattern suggests that microorganisms intensified the mining of native soil nutrients to obtain carbon sources commensurate with the surplus nitrogen. Consequently, the conversion efficiency of root-derived carbon into stable SOC and the retention of nutrients in the rhizosphere may face a risk of decline [63]. The suppression of lignin degradation by high nitrogen is consistent with classic findings in litter decomposition studies. In contrast, the sustained net nitrogen release from TR under high nitrogen has rarely been reported in fine root decomposition research and may represent a feature specific to the functional differentiation of crop roots.

4.3. Differences in Dominant Drivers and Regulatory Pathways Between the Two Root Types

Identifying the dominant drivers of root decomposition helps clarify the cascading mechanisms regulating decomposition pathways. Although AR and TR differ markedly in functional identity and morphological structure, their decomposition shares several common drivers. First, exogenous nitrogen affected *K* in both root types mainly through indirect pathways (Table S13), acting primarily via the soil module. Previous studies suggest that this indirect effect operates mainly through the extracellular enzyme system [51]. Second, microbial processes may serve as a common mediator of decomposition in both root types [64], and this study provides indirect evidence for one specific mechanism. The structural equation model showed a consistently significant negative association between the soil module and *K* in both root types (Figure 5). One plausible explanation is that higher soil nutrient availability reduces the microbial demand for nitrogen mining from litter, thereby lowering the relative value of root litter as a nutrient substrate [65]. This result is consistent with the prediction of the microbial nitrogen mining theory. More broadly, regardless of substrate quality, microbial nitrogen assimilation and immobilization, resource allocation priorities for extracellular enzyme synthesis, and adaptive responses to C/N stoichiometric imbalance may all mediate the temporal dynamics of *K*. Third, climatic factors constitute the fundamental driving force of decomposition [66]. Temperature and precipitation act throughout the entire decomposition process by influencing enzymatic reaction rates and microbial metabolic activity.

Nevertheless, the dominant driving pathways of the two root types diverged considerably. For AR, morphological plasticity was the leading factor explaining decomposition variation, accounting for 47.7% at the module level ($p = 0.001$), and the direct path from the morphology module to *K* was significant ($\beta = 0.62$, $p < 0.001$). The indirect effect of climate on *K* through the morphology module was also significant (Table S13). A plausible mechanism is that external factors promoted rapid disintegration of cortical tissues and increased SRA, which enhanced substrate accessibility and reduced the diffusion resistance to microbial hyphal invasion and enzyme penetration, ultimately regulating *K* indirectly [12,67]. This indicates that, for high-quality litter, the dynamic evolution of morphological traits has greater predictive power for *K* than initial stoichiometric characteristics [68,69]. In contrast, the direct effect of the nutrient release module on *K* was not significant for AR (Figure 5a). This suggests that nutrient release is more likely a concomitant outcome of rapid AR decomposition than a direct driver of *K*. Notably, the net nitrogen enrichment and relative lignin concentration in root residues during later decomposition (Figure 2c,f) suggest a trend toward substrate recalcitrance. This asynchrony between carbon and nitrogen loss may constrain decomposition persistence through negative feedback [65,70,71]. For TR, the climatic module was the primary source of decomposition variation, accounting for 54.2% at the module level, with a significant direct path to *K* ($\beta = 1.64$, $p < 0.001$). This is mainly because TR are subject to limited enzyme accessibility from the onset of decomposition. Under these conditions, direct regulation of enzymatic reactions by temperature, together

with moisture-driven mass transfer at the substrate-microbe interface, becomes the key rate-limiting step of decomposition. In addition, the nutrient release module exerted a significant positive direct effect on *K* in TR, in sharp contrast to AR (Figure 5b). Soil total nitrogen and climatic factors jointly formed the main driving axis. The former supplies nitrogen for the microbial synthesis of degradative enzymes, whereas the latter influences the rate of enzymatic reactions [72]. Together, they provide the conditions for overcoming the enzymatic bottleneck imposed by the recalcitrant substrates of TR. Taken together, the two root types exhibited a divergent pattern in which the decomposition of AR is dominated by the morphological channel, whereas the decomposition of TR is dominated by the nutrient mineralization channel. This pattern echoes the evidence for the decoupling of morphological and chemical traits in the RES [68] and provides empirical support for incorporating root functional identity into decomposition models.

4.4. Agroecological Implications of Cotton Root Decomposition and Nitrogen Fertilizer Optimization

Crop nutrient return has become a key process in maintaining soil fertility [15,16], and quantitative assessment of root nutrient return is of practical significance for farmland nutrient management [73]. Based on the divergence described above, the nutrient return functions of the two root types can be quantitatively estimated as follows. However, direct observational data on the in situ differentiation and turnover parameters of cotton AR and TR remain scarce. To address this gap, the present study applied the root-order functional classification framework [74,75] and extrapolated from field observations. The average standing biomass of cotton fine roots (<2 mm) during the growing season was approximately 0.044 g·cm^{-3}, converted from data in this study, with an annual turnover rate of 0.61–0.88 [33,76]. AR and TR accounted for approximately 60–70% and 30–40% of total fine root biomass, respectively. Accordingly, the seasonal input of AR and TR litter to soil was approximately 0.016–0.027 and 0.008–0.016 g·cm^{-3}, respectively. Assuming root carbon and nitrogen contents of approximately 45% and 1.5% [77,78], AR returned approximately 0.007–0.012 g·cm^{-3} of carbon and 2.44×10^{-4}–4.10×10^{-4} g·cm^{-3} of nitrogen, whereas TR returned approximately 0.004–0.007 g·cm^{-3} of carbon and 1.22×10^{-4}–2.35×10^{-4} g·cm^{-3} of nitrogen. Combined with the results of this study, the carbon fractions and phosphorus returned by AR are released rapidly in the short term (Figure 2) and may promote the release of nutrients bound in native soil organic matter and in microbial turnover through a priming effect [12]. In addition, because nitrogen in AR litter is mainly retained through net immobilization during early decomposition (Figure 2c), net nitrogen return may be delayed and may subsequently serve as a potential nutrient supplement for cotton field soil. In contrast, the sustained nutrient release from TR under high nitrogen may provide a potential pathway for nutrient carryover across years in cotton fields [33].

As a key management practice for coordinating the functions of the two root litter types, the rate of nitrogen fertilization can potentially regulate both the magnitude and direction of the priming effect induced by root decomposition [79]. In this study, the promotion of AR decomposition by nitrogen addition was already evident at the lowest nitrogen addition rate (N1), whereas the decomposition of TR accelerated markedly only under high nitrogen (N3), mainly through enhanced cellulose degradation with lignin degradation suppressed (Figure 2). These results indicate that AR decomposition is more sensitive to nitrogen input, and that moderate nitrogen addition can effectively promote early nutrient release. By contrast, TR decomposition depends more on the gradual action of time and soil biological processes, and excessive nitrogen application may weaken its long-term contribution to soil carbon pool stability by inhibiting the lignin-degrading enzyme system. Accordingly, in intensive cropping systems with a high proportion of root return, nitrogen fertilizer management may need to account for the differential responses of the two root functional

identities and prioritize the rapid nutrient return function of AR. The nitrogen optimization implications proposed in this study should therefore be regarded as potential insights that require verification through experiments combining in situ root labeling with multiple sites, multiple seasons, and direct microbiological evidence.

5. Conclusions

Based on an in situ decomposition experiment with cotton AR and TR under different nitrogen application gradients, this study demonstrated that AR decompose rapidly and release nutrients early. Their decomposition variation was mainly explained by dynamic changes in morphological traits, and their decomposition was highly sensitive to nitrogen input, with significant promotion already occurring at the lowest nitrogen addition rate. In contrast, TR followed a structurally conservative, slow-turnover decomposition pattern, with climatic factors as the primary driver of decomposition variation. These results reveal the cascading regulatory mechanisms underlying cotton root litter decomposition from the perspective of root-order functional differentiation, providing a new decomposition-based perspective for nitrogen fertilization and residue management in croplands. However, this study was based on short-term decomposition observations and has several limitations. In particular, data on microbial community dynamics and extracellular enzyme functional changes during decomposition were lacking, so the complete mechanistic chain of nitrogen regulation remains to be fully elucidated, and the actual effects of root decomposition on aboveground crop growth require further evaluation. Future studies should therefore combine stable isotope tracing with long-term field observations to systematically resolve the dynamic response patterns of decomposition across different root functional types and their cascading effects on soil carbon and nitrogen cycling, thereby providing a more comprehensive theoretical framework for coordinated carbon and nutrient management in agroecosystems.

Supplementary Materials: The following supporting information can be downloaded at: https://www.mdpi.com/article/10.3390/agronomy16222329/s1, Figure S1: Dynamics of litter morphological traits in absorptive (AR) and transport roots (TR) during decomposition under nitrogen treatments. Figure S2: Dynamics of soil properties during litter decomposition under nitrogen treatments. Table S1: Three-way ANOVA of the effects of root type, sampling time and nitrogen treatment on residual biomass. Table S2: Assumption tests for decomposition analyses. Table S3: Eigenvalues and variance explained by the principal components. Table S4: Pearson correlation matrix of the root traits used in the PCA. Table S5: Fixed-effect coefficients of the linear mixed-effects model for *K*. Table S6: Shapiro–Wilk normality tests for the variables used in the LMM-ANCOVA and hierarchical partitioning analyses. Table S7: Estimated marginal means of z-standardized *K* by nitrogen rate and root type. Table S8: Module-level hierarchical partitioning of the variation in *K*. Table S9: Single-layer hierarchical partitioning of the variation in *K*. Table S10: Variance inflation factors of the indicators in the single-layer hierarchical partitioning. Table S11: Coefficients of determination of the piecewise SEM submodels. Table S12: Variance inflation factors of the predictors in the piecewise SEM submodels. Table S13: Bootstrap indirect effects of N addition and climate on *K* in the piecewise SEMs. Table S14: Tests of directed separation (d-separation) for the omitted direct path from N rate to *K*. Table S15: Loadings of the measured variables on the first principal component of each module.

Author Contributions: Conceptualization, Y.H. and X.P.; methodology and formal analysis, Y.H. and H.W.; curation, M.L. and X.L.; writing—original draft preparation and writing—review and editing, Y.H.; visualization, Z.S. and Q.Z.; supervision, W.Z.; funding acquisition, X.P.; All authors have read and agreed to the published version of the manuscript.

Funding: This study was funded by the National Natural Science Foundation of China (32460538), Xinjiang Production and Construction Corps Science and Technology Program (2024DB015) and Xinjiang Production and Construction Corps Guiding Science, Technology Program (2023ZD049).

Data Availability Statement: The datasets generated and analysed during the current study are available from the corresponding author on reasonable request. The original dataset being part of a larger research project conducted by the authors' group and also containing data related to other ongoing studies that have not yet been published.

Acknowledgments: We thank the staff of the Agronomy Experimental Farm of Shihezi University, Shihezi City, Xinjiang Uygur Autonomous Region, China, for their help during data collection and the laboratory staff for their guidance during data analysis.

Conflicts of Interest: The authors declare no conflicts of interest.

Abbreviations

The following abbreviations are used in this manuscript:

TNC	Total non-structural carbohydrates
N	Litter total nitrogen
C	Litter total carbon
P	Litter total phosphorus
AD	Root average diameter
SRL	Specific root length
SRA	Specific root area
RTD	Root tissue density
SEI	The soil enzyme activity index
NT	Nitrogen treatment
Soil P	Soil total phosphorus
Soil N	Soil total nitrogen
SOC	Soil organic carbon

References

1. Zheng, H.P.; Yang, T.J.; Bao, Y.Z.; He, P.P.; Yang, K.M.; Mei, X.L.; Wei, Z.; Xu, Y.C.; Shen, Q.R.; Banerjee, S. Network analysis and subsequent culturing reveal keystone taxa involved in microbial litter decomposition dynamics. *Soil Biol. Biochem.* **2021**, *157*, 108230. [CrossRef]
2. Su, Z.X.; Su, B.Q.; Shangguan, Z.P. Advances in Effects of Plant Litter Decomposition on the Stability of Soil Organic Carbon. *Res. Soil Water Conserv.* **2022**, *29*, 406–413. [CrossRef]
3. Dong, L.L.; Berg, B.; Luo, Y.Q.; Zou, H.T.; Sun, T. Time-varying associations between absorptive fine roots and leaf litter decomposition across 23 plant species. *Soil Biol. Biochem.* **2025**, *204*, 109751. [CrossRef]
4. Zheng, J.J.; Freschet, G.T.; Tedersoo, L.; Li, S.G.; Yan, H.; Jiang, L.; Wang, H.M.; Ma, N.; Dai, X.Q.; Fu, X.L.; et al. A trait-based root acquisition-defence-decomposition framework in angiosperm tree species. *Nat. Commun.* **2024**, *15*, 5311. [CrossRef]
5. Freschet, G.T.; Aerts, R.; Cornelissen, J.H.C. A plant economics spectrum of litter decomposability. *Funct. Ecol.* **2012**, *26*, 56–65. [CrossRef]
6. Birouste, M.; Kazakou, E.; Blanchard, A.; Roumet, C. Plant traits and decomposition: Are the relationships for roots comparable to those for leaves? *Ann. Bot.* **2012**, *109*, 463–472. [CrossRef]
7. Pregitzer, K.S.; DeForest, J.L.; Burton, A.J.; Allen, M.F.; Ruess, R.W.; Hendrick, R.L. Fine root architecture of nine North American trees. *Ecol. Monogr.* **2002**, *72*, 293–309. [CrossRef]
8. Keel, S.G.; Campbell, C.D.; Högberg, M.N.; Richter, A.; Wild, B.; Zhou, X.H.; Hurry, V.; Linder, S.; Näsholm, T.; Högberg, P. Allocation of carbon to fine root compounds and their residence times in a boreal forest depend on root size class and season. *New Phytol.* **2012**, *194*, 972–981. [CrossRef]
9. Zhou, M.; Guo, Y.M.; Sheng, J.; Yuan, Y.J.; Zhang, W.H.; Bai, W.M. Using anatomical traits to understand root functions across root orders of herbaceous species in a temperate steppe. *New Phytol.* **2022**, *234*, 422–434. [CrossRef]
10. Sanaei, A.; van der Plas, F.; Chen, H.M.; Davids, S.; Eckhardt, S.; Hennecke, J.; Kahl, A.; Möller, Y.; Richter, R.; Schütze, J.; et al. Tree growth is better explained by absorptive fine root traits than by transport fine root traits. *Commun. Biol.* **2025**, *8*, 313. [CrossRef]
11. Mao, Z.; Roumet, C.; Rossi, L.M.W.; Merino-Martín, L.; Nespoulous, J.; Taugourdeau, O.; Boukcim, H.; Fourtier, S.; Del Rey-Granado, M.; Ramel, M.; et al. Intra- and inter-specific variation in root mechanical traits for twelve herbaceous plants and their link with the root economics space. *Oikos* **2023**, *2023*, e09032. [CrossRef]
12. Wei, L.; Zhang, S.S.; Li, J.B.; Niu, C.Y.; Xu, H.X.; Yao, P.W.; Shou, W.K. Absorptive rather than transport root decomposition drives soil carbon sequestration: A case study of *Platycladus orientalis* and *Quercus variabilis*. *Geoderma* **2022**, *428*, 116186. [CrossRef]

13. Zhao, X.X.; Tian, Q.X.; Michelsen, A.; Lin, Q.L.; Yuan, X.D.; Chen, L.; Lu, M.Z.; Jiang, Q.H.; Zhao, R.D.; Liu, F. Home-field advantage of litter decomposition differs among leaves, absorptive roots, and transport roots. *Plant Soil* **2024**, *500*, 391–402. [CrossRef]
14. Yin, L.M.; Zhang, T.S.; Dijkstra, F.A.; Huo, C.F.; Wang, P.; Cheng, W.X. Priming effect varies with root order: A case of Cunninghamia lanceolata. *Soil Biol. Biochem.* **2021**, *160*, 108354. [CrossRef]
15. Fulton-Smith, S.; Cotrufo, M.F. Pathways of soil organic matter formation from above and belowground inputs in a Sorghum bicolor bioenergy crop. *Glob. Change Biol. Bioenergy* **2019**, *11*, 971–987. [CrossRef]
16. Cai, M.M.; Chen, H.M.; Tan, H.; Chen, J.X.; He, S.B.; Long, M.X. Temporal dynamics of nutrient release from mulching of legume roots and shoots litter driven by microbial community during decomposition in organic orchards. *BMC Plant Biol.* **2025**, *25*, 374. [CrossRef]
17. Li, J.; Cheng, R.M.; Zhang, M.; Zhou, Y.W.; Chen, T.; Shen, Y.F.; Zeng, L.X.; Liu, C.F.; Xiao, W.F. Nitrogen and Phosphorus Additions Suppress Soil Respiration in Pinus Massoniana Plantations: Integrated Effects of Soil Chemistry, Microbial, Arthropod, and Litter on Carbon Release. *J. Soil Sci. Plant Nutr.* **2025**, *25*, 9579–9595. [CrossRef]
18. Yue, K.; Fornara, D.A.; Li, W.; Ni, X.Y.; Peng, Y.; Liao, S.; Tan, S.Y.; Wang, D.Y.; Wu, F.Z.; Yang, Y.S. Nitrogen addition affects plant biomass allocation but not allometric relationships among different organs across the globe. *J. Plant Ecol.* **2021**, *14*, 361–371. [CrossRef]
19. Hou, S.L.; Hättenschwiler, S.; Yang, J.J.; Sistla, S.; Wei, H.W.; Zhang, Z.W.; Hu, Y.Y.; Wang, R.Z.; Cui, S.Y.; Lü, X.T.; et al. Increasing rates of long-term nitrogen deposition consistently increased litter decomposition in a semi-arid grassland. *New Phytol.* **2021**, *229*, 296–307. [CrossRef]
20. Su, Y.; Le, J.J.; Han, W.X.; Wang, C.H.; Li, K.H.; Liu, X.J. Long-term nitrogen addition consistently decreased litter decomposition rates in an alpine grassland. *Plant Soil* **2022**, *479*, 495–509. [CrossRef]
21. Wu, J.J.; Zhang, H.; Cheng, X.L.; Liu, G.H. Nitrogen addition stimulates litter decomposition rate: From the perspective of the combined effect of soil environment and litter quality. *Soil Biol. Biochem.* **2023**, *179*, 108992. [CrossRef]
22. Yang, J.J.; Yang, Z.B.; Zhang, R.Z.; Guan, P.T.; Xu, T.H.; Tang, Y.; Ren, G.L. Litter quality outweighs climate in driving grassland root decomposition. *Front. Plant Sci.* **2025**, *16*, 1639369. [CrossRef]
23. Cui, J.; Zhu, Z.K.; Xu, X.L.; Liu, S.L.; Jones, D.L.; Kuzyakov, Y.; Shibistova, O.; Wu, J.S.; Ge, T.D. Carbon and nitrogen recycling from microbial necromass to cope with C:N stoichiometric imbalance by priming. *Soil Biol. Biochem.* **2020**, *142*, 107720. [CrossRef]
24. Alam, I.; Zhang, H.Y.; Du, H.; Rehman, N.U.; Manghwar, H.; Lei, X.; Khan, Z.; Batool, K.; Ge, L.F. Bioengineering Techniques to Improve Nitrogen Transformation and Utilization: Implications for Nitrogen Use Efficiency and Future Sustainable Crop Production. *J. Agric. Food Chem.* **2023**, *71*, 3921–3938. [CrossRef]
25. de Oliveira, J.D.; de Freitas, I.C.; Ferreira, E.A.; Duarte, A.C.S.; Ribeiro, J.M.; Barbosa, D.L.D.; Oliveira, W.R.; Signor, D.; Gontijo, M.M.; Teixeira, E.C.; et al. Spatial Pattern of Litter Decomposition and Soil Carbon and Nitrogen Stocks in an Agrosilvopastoral System in the Cerrado Biome. *J. Soil Sci. Plant Nutr.* **2026**, *26*, 2115–2129. [CrossRef]
26. Mao, S.C.; Li, P.C.; Chen, S.X.; Zhang, Z.G.; Li, X.; Tian, L.W.; Gao, L.; Wang, Z.B. Achievements, contributions, experiences, and perspective of cotton production in Xinjiang Oasis—On the occasion of the 70th anniversary of the establishment of the Xinjiang Uygur AutonomousRegion. *China Cotton* **2025**, *52*, 1–17.
27. Er, C.; Lin, T.; Xia, W.; Zhang, H.; Xu, G.Y.; Tang, Q.X. Coupling effects of irrigation and nitrogen levels on yield, water distributionand nitrate nitrogen residue of machine-harvested cotton. *Acta Agron. Sin.* **2022**, *48*, 497–510. [CrossRef]
28. Le, J.J.; Su, Y.; Peng, Q.W.; Geng, F.Z.; Han, W.X.; Li, W.L.; Li, K.H.; Liu, X.J. Effects of nitrogen addition on soil enzyme activities and ecoenzymaticstoichiometry in alpine grassland of the Tianshan Mountains. *Arid Zone Res.* **2020**, *37*, 382–389. [CrossRef]
29. Kost, E.; Kundel, D.; Barthel, M.; Conz, R.F.; Werner, R.A.; Ghiasi, S.; Bublitz, T.A.; Mäder, P.; Krause, H.M.; Six, J.; et al. Drought increases root and rhizodeposition carbon inputs into soils. *Plant Soil* **2026**, *519*, 103–127. [CrossRef]
30. Coker, H.R.; Lin, H.A.; Shackelford, C.E.B.; Tfaily, M.M.; Smith, A.P.; Howe, J.A. Drought stimulates root exudation of organic nitrogen in cotton (*Gossypium hirsutem*). *Front. Plant Sci.* **2024**, *15*, 1431004. [CrossRef]
31. Dong, X.X.; Zhang, Z.Y.; Wang, S.M.; Shen, Z.H.; Pu, X.Z. Morphological and physiological response of different root orders to biochar addition in continuous cropping cotton in Xinjiang, China. *Chin. J. Appl. Environ. Biol.* **2022**, *28*, 1430–1436. [CrossRef]
32. Guo, J.Q.; Chang, W.Z.; Hou, Z.A.; Li, J.H. Effect of N Rates on N Uptake Accumulation and Yield of Cotton under Drip Irrigation and Mulch. *J. Arid Land Resour. Environ.* **2008**, *22*, 139–142. [CrossRef]
33. Ren, A.T.; Lu, W.H.; Yang, J.J.; Ma, C.H. Seasonal change patterns in the production and mortality of fine roots in cotton and alfalfa. *Acta Pratacult. Sin.* **2015**, *24*, 213–219.
34. Guo, D.L.; Xia, M.X.; Wei, X.; Chang, W.J.; Liu, Y.; Wang, Z.Q. Anatomical traits associated with absorption and mycorrhizal colonization are linked to root branch order in twenty-three Chinese temperate tree species. *New Phytol.* **2008**, *180*, 673–683. [CrossRef]
35. Li, J.L.; Le, X.G.; Chen, X.P.; Reich, P.B.; Niklas, K.J.; Li, X.Q.; Wu, P.P.; Zhou, Y.J.; Zhong, Q.L.; Hu, D.D.; et al. Divergent intra- and interspecific root order variability identifies a two-dimensional root economics spectrum. *Plant Soil* **2024**, *499*, 473–490. [CrossRef]

36. Chen, S.M.; Li, M.S.; Gao, C.; Zhao, Y.L.; Hao, Z.W. Analysis on Fractal Characteristics of Barreled Cotton Root System Architecture. *J. Irrig. Drain.* **2015**, *34*, 75–79. [CrossRef]
37. Bao, S.D. *Soil and Agricultural Chemical Analysis*, 3rd ed; Agriculture Press: Beijing, China, 2000.
38. Wang, W. Biological Responses of Different Soybean Varieties to Low Potassiun Stress and Mechanism of Tolerance. Ph.D. Thesis, Shenyang Agricultural University, Shenyang, China, 2008.
39. Liu, Z.D.; Song, Y.Y.; Ma, X.Y.; Yuan, J.B.; Lou, Y.J.; Yang, C.; Tang, H.R.; Song, C.C. Deep soil microbial carbon metabolic function is important but often neglected: A study on the Songnen Plain reed wetland, Northeast China. *Fundam. Res.* **2023**, *3*, 833–843. [CrossRef]
40. Chang, C.; Cheng, J.L.; Qiang, S.; Song, X.L.; Zhang, Y. Methods for determination of stem lignin content and lignification of Solidago canadensis. *Plant Physiol. J.* **2018**, *54*, 917–924. [CrossRef]
41. Olson, J.S. Energy storage and the balance of producers and decomposers in ecological systems. *Ecology* **1963**, *44*, 322–331. [CrossRef]
42. Harmon, M.E.; Silver, W.L.; Fasth, B.; Chen, H.; Burke, I.C.; Parton, W.J.; Hart, S.C.; Currie, W.S.; Lidet. Long-term patterns of mass loss during the decomposition of leaf and fine root litter: An intersite comparison. *Glob. Change Biol.* **2009**, *15*, 1320–1338. [CrossRef]
43. Li, Q.; Zhang, M.H.; Geng, Q.H.; Jin, C.S.; Zhu, J.Y.; Ruan, H.H.; Xu, X. The roles of initial litter traits in regulating litter decomposition: A "common plot" experiment in a subtropical evergreen broadleaf forest. *Plant Soil* **2020**, *452*, 207–216. [CrossRef]
44. Lugli, L.F.; Andersen, K.M.; Aragao, L.; Cordeiro, A.L.; Cunha, H.K.; Fuchslueger, L.; Meir, P.; Mercado, L.M.; Oblitas, E.; Quesada, C.A.; et al. Multiple phosphorus acquisition strategies adopted by fine roots in low-fertility soils in Central Amazonia. *Plant Soil* **2020**, *450*, 49–63. [CrossRef]
45. Lin, D.M.; Yang, S.F.; Dou, P.P.; Wang, H.J.; Wang, F.; Qian, S.H.; Yang, G.R.; Zhao, L.; Yang, Y.C.; Fanin, N. A plant economics spectrum of litter decomposition among coexisting fern species in a sub-tropical forest. *Ann. Bot.* **2020**, *125*, 145–155. [CrossRef]
46. Makita, N.; Fujii, S. Tree species effects on microbial respiration from decomposing leaf and fine root litter. *Soil Biol. Biochem.* **2015**, *88*, 39–47. [CrossRef]
47. Yu, Y.; Liu, L.; Zhao, J.N.; Wang, S.C.; Zhou, Y.J.; Xiao, C.W. The Diversity of Soil Bacteria and Fungi Under Altered Nitrogen and Rainfall Patterns in a Temperate Steppe. *Front. Microbiol.* **2022**, *13*, 906818. [CrossRef]
48. Jin, W.H.; Dong, H.Y.; Wu, Q.F.; Shao, S.; Liang, C.F.; Ma, X.M.; Li, Y.F.; Luo, Y.; Chen, J.H.; Qin, H. Microbial stoichiometric imbalance and community composition determine the priming effects caused by leaf litter input in a subtropical forest soil. *Plant Soil* **2025**, *515*, 1499–1516. [CrossRef]
49. Wang, D.; Wang, J.J.; Olatunji, O.A.; Liu, Q. Different decomposition metrics of root xylem and root tissues outside xylem: An 8-year-long root decomposition study in an alpine shrubland. *Plant Soil* **2021**, *463*, 415–425. [CrossRef]
50. Liang, L.Y.; Liu, W.X.; Jalaid, N.; Peng, Z.Y.; Guo, L.L.; Liu, L.L. A meta-analysis of enzyme activity responses to nitrogen addition during litter decomposition. *Geoderma* **2026**, *471*, 117887. [CrossRef]
51. Chen, X.; Cao, J.J.; Sinsabaugh, R.L.; Moorhead, D.L.; Bardgett, R.D.; Fanin, N.; Nottingham, A.T.; Zheng, X.H.; Chen, J. Soil extracellular enzymes as drivers of soil carbon storage under nitrogen addition. *Biol. Rev.* **2025**, *100*, 1716–1733. [CrossRef]
52. Cao, Y.S.; Zhao, F.L.; Zhao, R.D.; Ren, J.S.; Zhu, T.B.; Zhang, F. Impact of nitrogen addition on soil organic carbon across ecosystems: Microbial roles and environmental regulation. *Geoderma* **2025**, *461*, 117501. [CrossRef]
53. Fu, X.F.; Xu, C.H.; Geng, Q.H.; Ma, X.C.; Zhang, H.G.; Cai, B.; Hu, G.Q.; Xu, X. Effects of nitrogen application on the decomposition of fine roots in temperate forests: A meta-analysis. *Plant Soil* **2022**, *472*, 77–89. [CrossRef]
54. Pei, G.T.; Liu, J.; Peng, B.; Wang, C.; Jiang, P.; Bai, E. Nonlinear Coupling of Carbon and Nitrogen Release During Litter Decomposition and its Responses to Nitrogen Addition. *J. Geophys. Res.-Biogeosci.* **2020**, *125*, e2019JG005462. [CrossRef]
55. Wang, Y.X.; Wang, H.M.; Dai, X.Q.; Kou, L.; Meng, S.W.; Fu, X.L. Decoupled responses of leaf and root decomposition to nutrient deposition in a subtropical plantation. *Soil Biol. Biochem.* **2022**, *168*, 108643. [CrossRef]
56. Yu, W.Y.; Wang, C.W.; Cornelissen, J.H.C.; Ye, X.H.; Huang, Z.Y.; Wang, D.L.; Liu, G.F. Litter position and stoichiometry regulate plant litter decomposition and nitrogen release in terrestrial ecosystems. *Catena* **2025**, *256*, 109093. [CrossRef]
57. Li, Y.B.; Bezemer, T.M.; Yang, J.J.; Lu, X.T.; Li, X.Y.; Liang, W.J.; Han, X.G.; Li, Q. Changes in litter quality induced by N deposition alter soil microbial communities. *Soil Biol. Biochem.* **2019**, *130*, 33–42. [CrossRef]
58. Xing, A.J.; Shen, H.H.; Zhao, M.Y.; Fang, J.Y. Reversal of the Litter N Effect on Decomposition at Higher N Addition Rates. *J. Geophys. Res.-Biogeosci.* **2025**, *130*, e2024JG008570. [CrossRef]
59. Sun, T.; Hobbie, S.E.; Berg, B.; Zhang, H.G.; Wang, Q.K.; Wang, Z.W.; Hättenschwiler, S. Contrasting dynamics and trait controls in first-order root compared with leaf litter decomposition. *Proc. Natl. Acad. Sci. USA* **2018**, *115*, 10392–10397. [CrossRef]
60. Zheng, Y.; Hu, Z.K.; Pan, X.; Chen, X.Y.; Derrien, D.; Hu, F.; Liu, M.Q.; Hättenschwiler, S. Carbon and nitrogen transfer from litter to soil is higher in slow than rapid decomposing plant litter: A synthesis of stable isotope studies. *Soil Biol. Biochem.* **2021**, *156*, 108196. [CrossRef]

61. Xu, H.W.; Qu, Q.; Li, G.W.; Liu, G.B.; Geissen, V.; Ritsema, C.J.; Xue, S. Impact of nitrogen addition on plant-soil-enzyme C-N-P stoichiometry and microbial nutrient limitation. *Soil Biol. Biochem.* **2022**, *170*, 108714. [CrossRef]
62. Yan, G.Y.; Luo, X.; Liang, C.; Han, S.J.; Liu, G.C.; Yin, L.M.; Wang, X.C.; Zhang, Z.; Xu, L.J.; Xing, Y.J.; et al. Nitrogen deposition enhances soil organic carbon sequestration through plant-soil-microbe synergies. *J. Ecol.* **2025**, *113*, 2889–2904. [CrossRef]
63. Ye, Y.H.; Wu, Z.; Zhang, S.B.; Tong, L.C.; Huang, W.Q.; Cui, Z.P.; Han, Y.Y. Effects of nitrogen addition on SOC in alpine grasslands of the Qinghai-Tibetan Plateau and adjacent mountain regions: A meta-analysis. *Front. Environ. Sci.* **2025**, *13*, 1677328. [CrossRef]
64. Rocci, K.S.; Pierson, D.; Jevon, F.V.; Polussa, A.; Oliverio, A.M.; Bradford, M.A.; Reich, P.B.; Wieder, W.R. Integrating Microbial Community Data Into an Ecosystem-Scale Model to Predict Litter Decomposition in the Face of Climate Change. *Glob. Change Biol.* **2025**, *31*, e70352. [CrossRef]
65. Craine, J.M.; Morrow, C.; Fierer, N. Microbial nitrogen limitation increases decomposition. *Ecology* **2007**, *88*, 2105–2113. [CrossRef]
66. Joly, F.X.; Scherer-Lorenzen, M.; Hättenschwiler, S. Resolving the intricate role of climate in litter decomposition. *Nat. Ecol. Evol.* **2023**, *7*, 214–223. [CrossRef]
67. Wang, S.Y.; Wang, W.N.; Wang, S.Z.; Yang, L.X.; Gu, J.C. Intraspecific variations of anatomical, morphological and chemical traits in leaves and absorptive roots along climate and soil gradients: A case study with Ginkgo biloba and Eucommia ulmoides. *Plant Soil* **2021**, *469*, 73–88. [CrossRef]
68. Cornwell, W.K.; Cornelissen, J.H.C.; Amatangelo, K.; Dorrepaal, E.; Eviner, V.T.; Godoy, O.; Hobbie, S.E.; Hoorens, B.; Kurokawa, H.; Pérez-Harguindeguy, N.; et al. Plant species traits are the predominant control on litter decomposition rates within biomes worldwide. *Ecol. Lett.* **2008**, *11*, 1065–1071. [CrossRef]
69. Wen, Z.H.; Shen, J.B. Rethinking the root economics space: Toward an integrative framework. *Trends Ecol. Evol.* **2026**, *41*, 583–585. [CrossRef]
70. Saha, S.; Huang, L.; Khoso, M.A.; Wu, H.B.; Han, D.H.; Ma, X.; Poudel, T.R.; Li, B.; Zhu, M.R.; Lan, Q.R.; et al. Fine root decomposition in forest ecosystems: An ecological perspective. *Front. Plant Sci.* **2023**, *14*, 1277510. [CrossRef]
71. See, C.R.; McCormack, M.L.; Hobbie, S.E.; Flores-Moreno, H.; Silver, W.L.; Kennedy, P.G. Global patterns in fine root decomposition: Climate, chemistry, mycorrhizal association and woodiness. *Ecol. Lett.* **2019**, *22*, 946–953. [CrossRef]
72. Jiang, L.; Wang, H.M.; Li, S.G.; Fu, X.L.; Dai, X.Q.; Yan, H.; Kou, L. Mycorrhizal and environmental controls over root trait-decomposition linkage of woody trees. *New Phytol.* **2021**, *229*, 284–295. [CrossRef]
73. Yuan, H.L.; Zhneg, T.T.; Lin, J.M.; Bao, X.L.; Min, K.K.; Zhu, X.F.; Xie, H.T.; Liao, C. Effect of agricultural and forest soil replacement on decomposition processes of plant residues. *Chin. J. Ecol.* **2024**, *43*, 1017–1024. [CrossRef]
74. Gu, J.C.; Wang, D.N.; Xia, X.X.; Wang, S.Z. Applications of functional classification methods for tree fine root biomass estimation: Ad-vancements and synthesis. *Chin. J. Plant Ecol.* **2016**, *40*, 1344–1351. [CrossRef]
75. McCormack, M.L.; Dickie, I.A.; Eissenstat, D.M.; Fahey, T.J.; Fernandez, C.W.; Guo, D.L.; Helmisaari, H.S.; Hobbie, E.A.; Iversen, C.M.; Jackson, R.B.; et al. Redefining fine roots improves understanding of below-ground contributions to terrestrial biosphere processes. *New Phytol.* **2015**, *207*, 505–518. [CrossRef]
76. Hai, X.Y.; Zhang, Z.; Ma, G.X.; Ma, L.L.; Lv, X. Growth and Senescence of Fine Roots of Cotton under Drip Irrigation Differ from Those under Flooding Irrigation. *J. Irrig. Drain.* **2017**, *36*, 1–6. [CrossRef]
77. Iversen, C.M.; McCormack, M.L.; Powell, A.S.; Blackwood, C.B.; Freschet, G.T.; Kattge, J.; Roumet, C.; Stover, D.B.; Soudzilovskaia, N.A.; Valverde-Barrantes, O.J.; et al. A global Fine-Root Ecology Database to address below-ground challenges in plant ecology. *New Phytol.* **2017**, *215*, 15–26. [CrossRef]
78. Freschet, G.T.; Pagès, L.; Iversen, C.M.; Comas, L.H.; Rewald, B.; Roumet, C.; Klimesová, J.; Zadworny, M.; Poorter, H.; Postma, J.A.; et al. A starting guide to root ecology: Strengthening ecological concepts and standardising root classification, sampling, processing and trait measurements. *New Phytol.* **2021**, *232*, 973–1122. [CrossRef]
79. Peng, Y.Z.; Biswas, A.; Adamowski, J.F.; Zhang, X.F.; Li, Y.M.; Li, L.; Peng, Y.Y.; Cao, J.J. Sources and stability of particulate organic matter (POM) and mineral-associated organic matter (MAOM) on the Loess Plateau: Implications for soil carbon management. *Ecol. Indic.* **2025**, *179*, 114162. [CrossRef]

Disclaimer/Publisher's Note: The statements, opinions and data contained in all publications are solely those of the individual author(s) and contributor(s) and not of MDPI and/or the editor(s). MDPI and/or the editor(s) disclaim responsibility for any injury to people or property resulting from any ideas, methods, instructions or products referred to in the content.